



# Imaging-based surrogate classification for risk stratification of hepatocellular carcinoma with microvascular invasion to adjuvant hepatic arterial infusion chemotherapy: a multicenter retrospective study

Lidi Ma, MD<sup>a,b</sup>, Cheng Zhang, MD<sup>a,b</sup>, Yuhua Wen, MD<sup>a,c</sup>, Kaili Xing, MD<sup>a,d</sup>, Shaohua Li, MD<sup>a,c</sup>, Zhijun Geng, MD<sup>a,b</sup>, Shuting Liao, MD<sup>a,b</sup>, Shasha Yuan, MD<sup>e</sup>, Xinming Li, MD<sup>f</sup>, Chong Zhong, MD<sup>g</sup>, Jing Hou, MD<sup>l</sup>, Jie Zhang, MD<sup>k</sup>, Mingyong Gao, MD<sup>l</sup>, Baojun Xu, MD<sup>h</sup>, Rongping Guo, MD<sup>a,c,\*</sup>, Wei Wei, MD<sup>a,c,\*</sup>, Chuanmiao Xie, MD<sup>a,b,\*</sup>, Lianghe Lu, MD<sup>a,c,\*</sup>

**Background:** Patients with microvascular invasion (MVI)-positive hepatocellular carcinoma (HCC) have shown promising results with adjuvant hepatic arterial infusion chemotherapy (HAIC) with FOLFOX after curative resection. The authors aim to develop an imaging-derived biomarker to depict MVI-positive HCC patients more precisely and promote individualized treatment strategies of adjuvant HAIC. **Materials and methods:** Patients with MVI-positive HCC were identified from five academic centers and utilized for model development (n = 470). Validation cohorts were pooled from a previously reported prospective clinical study conducted [control cohort (n = 145), adjuvant HAIC cohort (n = 143)] (NCT03192618). The primary endpoint was recurrence-free survival (RFS). Imaging features were thoroughly reviewed, and multivariable logistic regression analysis was employed for model development. Transcriptomic sequencing was conducted to identify the associated biological processes.

**Results:** Arterial phase peritumoral enhancement, boundary of the tumor enhancement, tumor necrosis stratification, and boundary of the necrotic area were selected and incorporated into the nomogram for RFS. The imaging-based model successfully stratified patients into two distinct prognostic subgroups in both the training, control, and adjuvant HAIC cohorts (median RFS, 6.00 vs. 66.00 months, 4.86 vs. 24.30 months, 11.46 vs. 39.40 months, all P < 0.01). Furthermore, no significant statistical difference was observed between patients at high risk of adjuvant HAIC and those in the control group (P = 0.61). The area under the receiver operating characteristic curve at 2 years was found to be 0.83, 0.84, and 0.73 for the training, control, and adjuvant HAIC cohorts, respectively. Transcriptomic sequencing analyses revealed associations between the radiological features and immune-regulating signal transduction pathways.

**Conclusion:** The utilization of this imaging-based model could help to better characterize MVI-positive HCC patients and facilitate the precise subtyping of patients who genuinely benefit from adjuvant HAIC treatment.

**Keywords:** hepatocellular carcinoma, imaging features, microvascular invasion, postoperative adjuvant hepatic arterial infusion chemotherapy, recurrence-free survival

<sup>a</sup>Collaborative Innovation Center for Cancer Medicine, State Key Laboratory of Oncology in South China, Guangdong Provincial Clinical Research Center for Cancer, Sun Yat-Sen University Cancer Center, <sup>b</sup>Department of Radiology, Sun Yat-sen University Cancer Center, State Key Laboratory of Oncology in South China, <sup>c</sup>Department of Liver Surgery, Sun Yat-sen University Cancer Center, <sup>d</sup>Department of Pathology, The First Affiliated Hospital, Sun Yat-sen University, <sup>f</sup>Department of Pathology, Zhujiang Hospital, Southern Medical University, <sup>g</sup>Department of Hepatobilliary Surgery, The First Affiliated Hospital of Guangzhou University of Chinese Medicine, <sup>h</sup>Department of Radiology, The First Affiliated Hospital of Jinan University, Guangzhou, <sup>h</sup>Department of Radiology, The First People's Hospital of Foshan, Foshan, Guangdong, <sup>h</sup>Department of Radiology, Hunan Cancer Hospital; Changsha and <sup>h</sup>Department of Radiology, Zhuhai People 's Hospital (Zhuhai hospital affiliated with Jinan University), Zhuhai, P.R China

L.M., C.Z., Y.W., K.X. contributed equally to this manuscript.

Sponsorships or competing interests that may be relevant to content are disclosed at the end of this article.

\*Corresponding author. Address: Department of Liver Surgery, Sun Yat-sen University Cancer Center, Guangzhou, 510060, P.R. China. Tel.: +20 873 431 54. E-mail: lulh@sysucc.org.cn (L. Lu); Department of Radiology, Sun Yat-sen University Cancer Center, Guangzhou, 510060, P.R. China. Tel.: +20 873 432 18. E-mail: xchuanm@sysucc.org.cn (C. Xie); Department of Liver Surgery, Sun Yat-sen University Cancer Center, Guangzhou, 510060, P.R. China. Tel.: +20 873 431 54. E-mail: weiwei@sysucc.org.cn (W. Wei); Department of Liver Surgery, Sun Yat-sen University Cancer Center, Guangzhou, 510060, P.R. China. Tel.: +20 873 431 54. E-mail: guorp@sysucc.org.cn (R. Guo).

Copyright © 2024 The Author(s). Published by Wolters Kluwer Health, Inc. This is an open access article distributed under the terms of the Creative Commons Attribution-Non Commercial-No Derivatives License 4.0 (CCBY-NC-ND), where it is permissible to download and share the work provided it is properly cited. The work cannot be changed in any way or used commercially without permission from the journal.

International Journal of Surgery (2025) 111:872-883

Received 22 March 2024; Accepted 24 June 2024

Supplemental Digital Content is available for this article. Direct URL citations are provided in the HTML and PDF versions of this article on the journal's website, www.lww.com/international-journal-of-surgery.

Published online 24 July 2024

http://dx.doi.org/10.1097/JS9.0000000000001903

#### Introduction

Hepatocellular carcinoma (HCC) is a highly prevalent malignancy and a leading cause of cancer-related mortality worldwide<sup>[1]</sup>. Although surgical resection remains the cornerstone of curative treatment, its long-term efficacy is hindered by an unsatisfactorily high recurrence rate ranging from 60 to  $70\%^{[2,3]}$ . Therefore, there exists a substantial clinical need in patients with HCC for adjuvant treatments aimed at preventing tumor recurrence.

The management of adjuvant treatment strategies in HCC poses a considerable challenge. Despite various adjuvant therapies being investigated to improve long-term survival, no standard treatment options are currently available [4,5]. This challenge is twofold: firstly, it involves identifying patients who truly require adjuvant therapy; and secondly, determining the most appropriate treatment approach to employ. Recently, our study has revealed that postoperative adjuvant hepatic arterial infusion chemotherapy (HAIC) based on FOLFOX represents a promising emerging treatment approach for HCC patients with microvascular invasion (MVI-positive), demonstrating a median recurrence-free survival (RFS) of 20.3 months compared to 10.0 months for patients receiving routine follow-up  $(NCT03192618)^{[6,7]}$ . Despite the hope brought by adjuvant HAIC in improving the dismal prognosis of HCC patients with MVI, several questions remain unresolved in clinical practice due to the heterogeneous characteristics observed in MVI-positive patients and the fact that not all cases relapse after curative resection<sup>[8,9]</sup>. The previously acclaimed success of MVI in guiding the treatment strategy of adjuvant HAIC in HCC patients has now reached a plateau. Thus, the identification of individual patients who would genuinely benefit from the adjuvant HAIC is an urgent imperative.

As an indispensable component of clinical practice, medical imaging plays a pivotal role in the management of tumors, with emerging evidence indicating that imaging-based features can provide valuable insights into molecular characteristics and genetic patterns, thereby complementing tumor heterogeneity and enhancing the predictive capabilities of existing models<sup>[10,11]</sup>. Previous studies have demonstrated that imaging features of HCC reflect the dynamic and physiological interplay of parenchymal cells, blood vessels, and stroma, which reflect different aggressive biological behaviors and hold great promise as an intermediate phenotype bridging the gap between genetic variation and pathology<sup>[12–14]</sup>. However, the ability of radiological imaging features to accurately reflect the heterogeneity among MVI-positive HCC patients remains uncertain, and it is yet to be determined whether the analysis of radiological characteristics can aid in postoperative adjuvant HAIC for MVI-positive patients.

Therefore, this study conducted a large multicenter cohort analysis to investigate and validate the potential of imaging characteristics in stratifying MVI-positive patients and guiding treatment strategies for postoperative adjuvant HAIC.

#### **Materials and methods**

#### Study patients

We analyzed patients with histologically confirmed HCC with MVI after resection between February 2009 and January 2022

#### **HIGHLIGHTS**

- In retrospective multicenter studies of hepatocellular carcinoma (HCC) patients with microvascular invasion (MVI-positive), the imaging-based model successfully stratified patients into two distinct prognostic subgroups, with areas under the receiver operating characteristic curve of 0.73–0.84.
- The imaging-based model successfully facilitated the precise subtyping of patients who genuinely benefit from adjuvant HAIC treatment (11.46 vs. 39.40 months, P < 0.01).
- Based on RNA-seq data analysis, this study uncovered that differentially expressed genes were found to commonly be involved in inflammatory response regulation, and immune regulation.

from 5 independent institutions in China (Sun Yat-sen University Cancer Center (SYSUCC), the First Affiliated Hospital of Sun Yat-sen University (AHSYSU), Hunan Cancer Hospital (HNCA), Zhuhai People's Hospital (ZHPH), and Zhujiang Hospital of Southern Medical University (ZJHSMU)) to produce the training cohort. A total of 2791 patients treated with hepatic resection and with pathologically proven HCC were screened for eligibility. Of these 2791 patients, only patients who met all the following criteria were enrolled in this study.

The main inclusion criteria were as follows: (i) age older than or equal to 18 years old; (ii) histologically confirmed HCC with MVI-positive after resection; (iii) no other anticancer treatments before surgery; (iv) an Eastern Cooperative Oncology Group performance status of  $\leq 2$ ; (v) without macrovascular invasion or distant metastasis; and (vi) without other malignant tumors. The main exclusion criteria were as follows: (i) without available computed tomography (CT) or magnetic resonance (MR) images for evaluation, (ii) with any other treatments before surgical resection; (iii) patients with histologically proven positive resection margin (R1 resection); (iv) recurrence 4-6 weeks after hepatectomy; (v) incomplete data or no follow-up data. The inclusion and exclusion criteria were consistent with our previously published prospective clinical trials (identifier: NCT03192618) except for those without available images for evaluation. In total, 470 HCC patients were enrolled (Fig. 1A).

The validation cohort was formed by screening the data of all patients from five centers SYSUCC, the First Affiliated Hospital of Guangzhou University of Chinese Medicine (AHGUCM), the First People's Hospital of Foshan (FPHP), ZJHSMU, and the First Affiliated Hospital of Jinan University (FAHJNU) who participated in our previous prospective clinical trials study (identifier: NCT03192618), conducted between March 2016 and June 2021. The same inclusion and exclusion criteria were applied to select patients for the validation cohort. Subsequently, the validation cohort comprised patients in the treatment group (n=143) who received adjuvant HAIC after hepatectomy, and the control group (n=145) consisting of patients who did not receive any adjuvant treatment following curative resection (Fig. 1B).

The flowchart depicting the methodology employed in this multicenter retrospective study is illustrated in Figure 1. This investigation received approval from the local Research Ethics Committees (B2021-214-Y02), and informed consent was duly

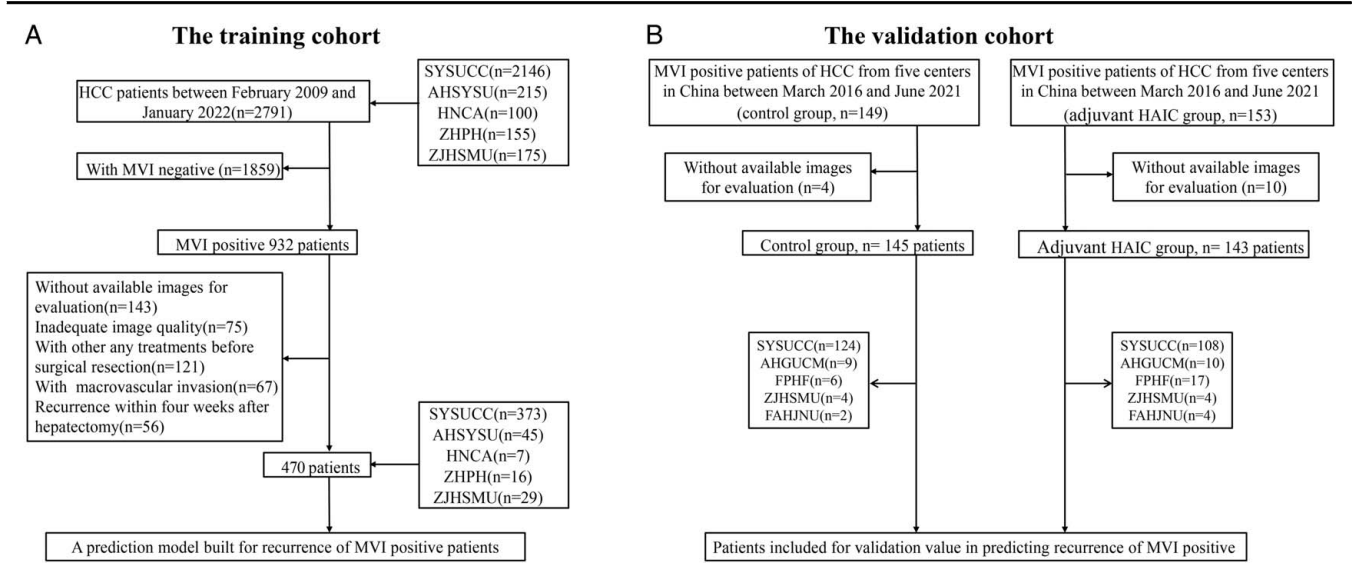


Figure 1. Flow chart of the study population. HAIC, hepatic arterial infusion chemotherapy; HCC, hepatocellular carcinoma; MVI, microvascular invasion; SYSUCC, Sun Yat-sen University Cancer Center; AHSYSU, the first Affiliated Hospital of Sun Yat-sen University; HNCA, Hunan Cancer Hospital; ZHPH, Zhuhai People's Hospital; ZJHSMU, Zhujiang Hospital of Southern Medical University; AHGUCM, the first Affiliated Hospital of Guangzhou University of Chinese Medicine; FPHF, the First People's Hospital of Foshan; FAHJNU, the First Affiliated Hospital of Jinan University.

waived from all participating patients due to the retrospective study. The work has been reported in line with the STROCSS criteria<sup>[15]</sup>. Supplemental Digital Content 1, http://links.lww.com/JS9/D49.

## Image acquisition

The CT protocol consisted of pre-contrast and dynamic contrast images, including the arterial phase (AP), portal venous phase (PVP), and delayed phase (DP). The contrast-enhanced MRI sequences consisted of T2-weighted imaging, dynamic T1-weighted imaging in the pre-contrast phase (AP, PVP, DP), and diffusion-weighted imaging (b = 50/800). The scanning protocols of CT and MR liver acquisition from different centers are shown in Table S1, Supplemental Digital Content 2, http://links.lww.com/JS9/D50 and S2, Supplemental Digital Content 2, http://links.lww.com/JS9/D50.

#### Clinical characteristics and image analysis

We obtained clinical characteristics from electronic health records, including age, gender, hepatitis B virus infection, liver cirrhosis, alpha-fetoprotein level (AFP), liver function, and Barcelona Clinic Liver Cancer stage (BCLC). The analysis of CT or MR image features was performed by two radiologists (LD Ma and C Zhang) who were blinded to the radiological reports and patient's follow-up data. In case of disagreement, a senior radiologist (CM Xie) resolved the discrepancies. All conflicting radiological characteristics were reviewed by the senior radiologist. The major features included the following: (a) tumor number, defined as solitary when the number equaled 1, otherwise defined as multiple when number greater than or equal to 2; (b) tumor size, defined as the largest outer-edge-to-outer-edge dimension on the transverse section; (c) AP enhancement type, including the following four types: types 1 (nonrim AP hyperenhancement (APHE), type 2 (rim APHE), type 3 (homogeneous enhancement), type 4 (without APHE); (d) AP enhancement degree, defined as type 1 when the area of maximum section for tumor enhancement was less than or equal to 50% otherwise defined as type 2; (e) internal or peripheral artery, defined as presence of discrete arterial enhancement within or around the tumor; (f) AP peritumoral enhancement, defined as hyperintensity or hyperdensity in the AP, which becomes isointensity or isodensity on the PVP or DP; (g) boundary of the tumor enhancement, defined as clear or obscure in AP; (h) nonperipheral washout, defined that apparent washout is not most pronounced in the periphery of the observation; (i) capsule appearance, defined as peripheral rim of uniform and smooth hyperenhancement in the PVP or DP, which is categorized into three groups (absent, incomplete, and complete); (i) tumor margin, defined according to the following four types: nodular with extranodular extension, multinodular confluent, infiltrative shaped tumor, smooth margin; (k) satellite nodules, defined as small (<2 cm) tumor nodules close (<2 cm) to the main tumor; (1) boundary of the necrotic area, classified as clear or obscure/without nonenhanced area; (m) tumor necrosis stratification, defined as type 1 when the area of maximum section for tumor necrosis is less than or equal to 40% otherwise defined as type 2; (n) intratumoral hemorrhage, defined as hyperdensity on pre-contrast CT or hyperintensity on pre-contrast MRI (Table S3, Supplemental Digital Content 2, http://links.lww.com/JS9/D50).

#### Follow-up

RFS was the primary endpoint, defined as the time interval from liver resection to initial tumor recurrence or last follow-up if no recurrence occurred. All patients underwent regular postoperative follow-up using serum alpha-fetoprotein and contrast-enhanced ultrasound, CT, or MRI every 2–3 months. Patients without recurrence or death at the time of data analysis were considered alive and event-free until their last follow-up date. Recurrence was confirmed based on cytologic/histologic evidence or noninvasive diagnostic criteria for HCC established by the European Association for the Study of Liver. This study was censored on 10 October 2021.

Table 1
Patient characteristics.

	Entire cohort	Training cohort	Control cohort	HAIC cohort (n = 143)	
Characteristic	(n = 758)	(n = 470)	(n = 145)		
Age (median [IQR])	51 [43, 60]	50 [41, 58]	54 [47, 63]	51 [42, 62]	< 0.00
Sex, n (%)					0.41
Male	670 (88.39)	420 (89.36)	128 (88.28)	122 (85.31)	
Female	88 (11.61)	50 (10.64)	17 (11.72)	21 (14.69)	
Position of the lesion, <i>n</i> (%)					0.533
Left lobe	192 (25.33)	119 (25.32)	32 (22.07)	41 (28.67)	
Right lobe	521 (68.73)	320 (68.09)	107 (73.79)	94 (65.73)	
Bilateral lobe	45 (5.94)	31 (6.60)	6 (4.14)	8 (5.59)	
Num, n (%)					0.95
Solitary	699 (92.22)	434 (92.34)	134 (92.41)	131 (91.61)	
Multiple	59 (7.78)	36 (7.66)	11 (7.59)	12 (8.39)	
Maximum diameter (median [IQR]), mm	58 [38, 88]	60 [39, 89]	56 [35, 82]	56 [35, 85]	0.336
Intratumoral hemorrhage, n (%)					0.00
Negative	635 (83.77)	407 (86.60)	109 (75.17)	119 (83.22)	
Positive	123 (16.23)	63 (13.40)	36 (24.83)	24 (16.78)	
Density, n (%)					< 0.00
Homogeneity	247 (32.59)	180 (38.30)	32 (22.07)	35 (24.48)	
Heterogeneity	511 (67.41)	290 (61.70)	113 (77.93)	108 (75.52)	
AP enhancement type, n (%)	, ,	,	, ,	, ,	0.218
Type 1	27 (3.56)	21 (4.47)	5 (3.45)	1 (0.70)	
Type 2	620 (81.79)	376 (80.00)	120 (82.76)	124 (86.71)	
Type 3	49 (6.46)	36 (7.66)	6 (4.14)	7 (4.90)	
Type 4	62 (8.18)	37 (7.87)	14 (9.66)	11 (7.69)	
Nonperipheral washout, <i>n</i> (%)	,	,	, ,	,	0.190
Negative	40 (5.28)	30 (6.38)	4 (2.76)	6 (4.20)	
Positive	718 (94.72)	440 (93.62)	141 (97.24)	137 (95.80)	
Capsule appearance, n (%)	,	,	, ,	,	< 0.00
Absent	511 (67.41)	317 (67.45)	79 (54.48)	115 (80.42)	
Incomplete	70 (9.23)	66 (14.04)	3 (2.07)	1 (0.70)	
Complete	177 (23.35)	87 (18.51)	63 (43.45)	27 (18.88)	
Satellite nodules, n (%)	( /	. ( )		( )	0.297
Negative	625 (82.45)	381 (81.06)	120 (82.76)	124 (86.71)	
Positive	133 (17.55)	89 (18.94)	25 (17.24)	19 (13.29)	
Tumor margin, n (%)	,	,	,	,	< 0.00
Nodular with extranudular extension	54 (7.12)	38 (8.09)	9 (6.21)	7 (4.90)	
Multinodular confluent	341 (44.99)	228 (48.51)	54 (37.24)	59 (41.26)	
Infiltrative shaped tumor	247 (32.59)	145 (30.85)	62 (42.76)	40 (27.97)	
Smooth margin	116 (15.30)	59 (12.55)	20 (13.79)	37 (25.87)	
AP peritumoral enhancement, <i>n</i> (%)	- ()	()	()	(=====)	0.009
Negative	457 (60.29)	300 (63.83)	72 (49.66)	85 (59.44)	2.000
Positive	301 (39.71)	170 (36.17)	73 (50.34)	58 (40.56)	
Tumor necrosis stratification, <i>n</i> (%)	(55)	(55)	- (-5.5.)	(.5.55)	0.079
Type 1	588 (77.57)	358 (76.17)	109 (75.17)	121 (84.62)	0.01
Type 2	170 (22.43)	112 (23.83)	36 (24.83)	22 (15.38)	

## Table 1 (Continued)

	Entire cohort	Training cohort	Control cohort	HAIC cohort	
Characteristic	(n = 758)	(n = 470)	(n = 145)	(n = 143)	
Boundary of the necrotic area, <i>n</i> (%)					0.014
Without nonenhanced area	334 (44.06)	194 (41.28)	63 (43.45)	77 (53.85)	
Clear	360 (47.49)	226 (48.09)	74 (51.03)	60 (41.96)	
Obscure	64 (8.44)	50 (10.64)	8 (5.52)	6 (4.20)	
AP enhancement degree, n (%)					< 0.001
Type 1	120 (15.83)	110 (23.40)	3 (2.07)	7 (4.90)	
Type 2	638 (84.17)	360 (76.60)	142 (97.93)	136 (95.10)	
Internal or peripheral artery, <i>n</i> (%)					0.362
Negative	336 (44.33)	203 (43.19)	62 (42.76)	71 (49.65)	
Positive	422 (55.67)	267 (56.81)	83 (57.24)	72 (50.35)	
Boundary of the tumor enhancement, <i>n</i> (%)					0.142
Clear	322 (42.48)	211 (44.89)	60 (41.38)	51 (35.66)	
Obscure	436 (57.52)	259 (55.11)	85 (58.62)	92 (64.34)	
AFP (median [IQR]), ng/ml	109.10 [8.15, 3035.75]	89.71 [7.99, 3764.00]	133.70 [10.40, 1924.00]	210.70 [6.76, 3681.50]	0.947
ALB (median [IQR]), g/I	42.50 [39.70, 44.98]	41.90 [39.30, 44.30]	43.60 [41.50, 45.60]	43.30 [40.60, 46.35]	< 0.001
TBIL (median [IQR]), µmol/I	13.20 [9.90, 17.10]	13.40 [10.20, 17.78]	12.20 [9.30, 15.90]	13.20 [9.30, 16.40]	0.070
HBsAg, n (%)					0.869
Negative	109 (14.38)	70 (14.89)	20 (13.79)	19 (13.29)	
Positive	649 (85.62)	400 (85.11)	125 (86.21)	124 (86.71)	
BCLC stage, n (%)					0.949
0	26 (3.43)	18 (3.83)	4 (2.76)	4 (2.80)	
A	589 (77.70)	365 (77.66)	112 (77.24)	112 (78.32)	
В	143 (18.87)	87 (18.51)	29 (20.00)	27 (18.88)	
Cirrhosis, n (%)					0.892
Negative	364 (48.02)	225 (47.87)	68 (46.90)	71 (49.65)	
Positive	394 (51.98)	245 (52.13)	77 (53.10)	72 (50.35)	
Follow-up time (median [IQR]), m	24.00 [8.00, 46.00]	27.00 [6.00, 55.00]	18.13 [8.73, 33.93]	23.00 [12.30, 35.65]	0.023
Status, n (%)	·	·		•	0.003
Non-recurrence	358 (47.23)	207 (44.04)	65 (44.83)	86 (60.14)	
Recurrence	400 (52.77)	263 (55.96)	80 (55.17)	57 (39.86)	

AP enhancement (APHE) types, type 1 (nonrim arterial phase hyperenhancement [APHE]), type 2 (rim APHE), type 3 (homogeneous enhancement), type 4 (without APHE); tumor necrosis stratification: type 1, the area of maximum section for tumor necrosis  $\leq$  40%; type 2, the area of maximum section for tumor enhancement  $\leq$  50%; type 2, the area of maximum section for tumor enhancement > 50%.

AFP, alpha-fetoprotein level; ALB, albumin; AP, arterial phase; BCLC, Barcelona Clinic Liver Cancer; HAIC, hepatic arterial infusion chemotherapy; IQR, interquartile range; TBIL, total bilirubin.

#### Statistical analysis

The statistical analyses were performed using R software (https:// www.r-project.org/, version 4.2.3). Continuous variables are presented as the means  $\pm$  SD, or median (interquartile range, IQR) based on their distribution normality. Categorical variables were expressed as counts (percentages). The intrareader agreement of the imaging features was evaluated by Cohen kappa coefficients or intraclass correlation coefficient (ICC) with 95% CI. The kappa coefficients or ICC were as follows: less than or equal to 0.20, slight agreement; 0.21-0.40, fair agreement; 0.46-0.60, moderate agreement; 0.61-0.80, substantial agreement; and 0.81-1.00, almost perfect agreement. Univariate analysis was performed using the Kaplan–Meier method and compared using the log-rank test. The cut-off values for the AP enhancement degree and necrosis stratification were determined using the "survminer" package in R. Multivariate analyses were carried out through Cox proportional hazard regression with the backwards Akaike information criterion (AIC) selection method. Hazard ratios (HR) and 95% CI were estimated to assess associations. Model performance was evaluated by the timedependent area under the receiver operating characteristic curve (tdAUROC). Considering the clinical importance of the predicted absolute RFS probability, we developed a nomogram based on the final multivariate model using the 'rms' package. Additionally, we performed calibration curve analysis and decision curve analysis (DCA). To stratify patients into high and lowrisk groups, we used the 50th percentiles of relative risk points from the training cohort according to the multivariate model. Kaplan-Meier curves were employed to estimate RFS for different risk groups and cohorts, with comparison conducted using a log-rank test. The constructed model was applied to the 61 patients included in the genomics study, in which the corresponding transcriptomic data were obtained from tissue samples. All reported P values were two-sided, and statistical significance was defined as *P* less than 0.05.

#### Results

#### Characteristics of the study patients

The study cohorts consisted of the training cohort (n = 470), the adjuvant HAIC cohort (n=143), and the control cohort (n=145). In the total patient population, preoperative MR examination was performed on 313 patients (41.29%), CT examination on 384 patients (50.66%), and both CT and MR examinations on 61 patients (8.05%). The majority of patients had hepatitis B virus infection, with proportions of 85.11% in the training cohort, 86.71% in the adjuvant HAIC cohort, and 86.21% in the control cohort; accounting for a total proportion of 85.62% across all cohorts combined. Detailed baseline characteristics can be found in Table 1. The median follow-up time was 27.00 (6.00-55.00) months in the training cohort, 23.00 (12.30-35.65) months in the adjuvant HAIC cohort, and 18.13 (8.73-33.93) months in the control cohort. Recurrence was recorded in 263 patients (55.96%) in the training cohort, 57 (39.86%) in the adjuvant HAIC cohort, and 80 (55.17%) in the control cohort. The early recurrence (<2 years) rates were 46.81% (220/470), 37.06% (53/143), and 51.72% (75/145) in the training, the adjuvant HAIC, and control cohorts, respectively. The treatment selection for recurrent HCC was determined by the multidisciplinary team, with a comprehensive consideration of the recurrence pattern, including tumor size, number, anatomical location, time to recurrence and reserve liver function.

#### Assessment of interobserver agreement

Interobserver agreement was moderate for tumor necrosis stratification (Cohen  $\kappa = 0.75$ ; 95% CI: 0.52–0.98), boundary of the necrotic area (Cohen  $\kappa = 0.70$ ; 95% CI: 0.53–0.88), arterial phase peritumoral enhancement (Cohen  $\kappa = 0.92$ , 95% CI: 0.81–1.00), and boundary of the tumor enhancement (Cohen  $\kappa = 0.72$ , 95% CI: 0.52–0.91). The interobserver agreement was substantial to almost perfect for other imaging features (Table S4, Supplemental Digital Content 2, http://links.lww.com/JS9/D50).

# Construction of the multivariate Cox proportional hazards regression model

After conducting univariable analysis on the training cohort, we identified several factors associated with RFS, including sex, age, maximum tumor diameter (mm), satellite nodules, tumor margin, internal or peripheral artery involvement, AP peritumoral enhancement, tumor necrosis stratification, boundary of the necrotic area, AP enhancement degree, boundary of the tumor enhancement, AFP levels, HBsAg status and BCLC stage (all P < 0.05). Subsequently employing a multivariate Cox proportional hazards regression model with backward AIC for variable selection process revealed four significant independent prognostic factors for predicting RFS: arterial phase peritumoral enhancement (HR = 2.33; 95% CI: 1.76-3.08; P < 0.001), boundary of the tumor enhancement (HR = 2.09; 95% CI: 1.56-2.80; P < 0.001), tumor necrosis stratification (HR = 1.72; 95% CI: 1.25–2.36; P = 0.001) and boundary of the necrotic area (HR = 1.81; 95% CI: 1.30–2.51; P < 0.001) (Table 2).

#### Prognostic nomogram for RFS

The nomogram (Fig. 2) was constructed to forecast the absolute probability of RFS for each individual, based on the aforementioned four independent prognostic factors. This enables personalized estimation of probabilities and highlights the significance of individual characteristics. The 2-year AUROC of the model constructed using the aforementioned variables for predicting RFS was 0.83 (95% CI, 0.79-0.87) in the training cohort, 0.84 (95% CI, 0.74–0.93) in the control cohort, and 0.73 (95% CI, 0.62-0.83) in the adjuvant HAIC cohort (Fig. 3A-C). Furthermore, the time-dependent AUROC of the model was calculated for each cohort over time as depicted in Figure 3D-F. The calibration curves of the nomogram demonstrated excellent concordance between the predicted RFS probability by the nomogram and the actual RFS proportion within each cohort (Figure S1A-C, Supplemental Digital Content 3, http://links.lww. com/JS9/D51). Additionally, DCA for evaluating the clinical utility of the nomogram is presented in Figure S1D-F, Supplemental Digital Content 3, http://links.lww.com/JS9/D51, revealing that utilizing this predictive tool provided greater net benefit compared to assuming all patients had recurred when threshold probability exceeded 0.1.

Table 2
Univariate and multivariate analyses of preoperative imaging findings in predicting recurrence.

	Univariate analysis		Multivariate analysis		
Characteristic	Hazard ratio	P	Hazard ratio	Р	
Sex	0.57 (0.35-0.90)	0.017	0.63 (0.39, 1.02)	0.058	
Age (> 50 vs.	0.76 (0.58-0.98)	0.037	0.77 (0.59, 1.00)	0.050	
≤50 years)					
Location	1.23 (0.73-2.06)	0.432			
Number	1.19 (0.77-1.84)	0.433			
Maximum tumor diameter (mm)	1.01 (1.003–1.01)	< 0.001	1.00 (0.99, 1.00)	0.132	
Density	1.11 (0.87-1.43)	0.404			
AP enhancement type	0.78 (0.38-1.6)	0.498			
Nonperipheral washout	1.31 (0.78-2.22)	0.306			
Capsule appearance	0.75 (0.52-1.09)	0.132			
Satellite nodules	1.79 (1.35–2.37)	< 0.001	1.38 (0.72, 2.67)	0.331	
Tumor margin	3.05 (1.7–5.45)	< 0.001	1.47 (0.81, 2.67)	0.201	
			1.34 (0.71, 2.52)	0.367	
			1.18 (0.60, 2.34)	0.629	
Internal or peripheral artery	1.62 (1.27–2.07)	< 0.001	1.22 (0.89, 1.67)	0.215	
AP peritumoral enhancement	3.20 (2.49–4.11)	< 0.001	2.33 (1.76, 3.08)	< 0.001	
Intratumoral hemorrhage	1.04 (0.72-1.49)	0.846			
Tumor necrosis stratification	2.29 (1.76–2.98)	< 0.001	1.72 (1.25, 2.36)	0.001	
Boundary of the necrotic	2.35 (1.74-3.17)	< 0.001	1.80 (1.30, 2.50)	< 0.001	
area			1.07 (0.85, 1.35)	0.560	
AP enhancement degree	0.68 (0.52-0.90)	0.006	1.14 (0.83, 1.55)	0.424	
Boundary of the tumor enhancement	2.83 (2.18–3.67)	< 0.001	2.09 (1.56, 2.80)	< 0.001	
AFP (ng/ml)	1.44 (1.13-1.84)	0.003	1.22 (0.94, 1.60)	0.136	
ALB (g/l)	0.99 (0.97-1.02)	0.642			
TBIL (µmol/l)	1.01 (1.00-1.02)	0.244			
HBsAg	1.41 (0.96–2.06)	0.080			
BCLC stage	2.51 (1.39-4.55)	0.002	0.98 (0.46, 2.10)	0.968	
			0.94 (0.60, 1.46)	0.777	
Cirrhosis	1.08 (0.84–1.38)	0.561			

AFP, alpha-fetoprotein level; ALB, albumin; AP, arterial phase; BCLC, Barcelona Clinic Liver Cancer; TBII., total bilimbin.

#### Postoperative recurrence risk in different groups

The median (95% CI) RFS was 23 (16–33) months in the training cohort, 11.16 (7.70–14.6) months in the control cohort, and 27.10 (10.85–43.28) months in the adjuvant HAIC cohort. Using a cut-off value of 133.45 derived from the model probability points at the 50th percentile in the training cohort, patients were stratified into the high-risk group (points ≥ 133.45) and the lowrisk group (points <133.45). The RFS curves between high-risk and low-risk groups showed significant statistical differences in the training cohort (median RFS: 6.00 vs. 66.00 months, P < 0.0001, Fig. 4A), the control cohort (median RFS: 4.86 vs. 24.30 months, P < 0.0001, Fig. 4B), as well as the adjuvant HAIC cohort (median RFS:11.46 vs. 39.40 months, P = 0.0017, Fig. 4C). The 1-year, 2-year, and 3-year RFS rate was significantly lower in the high-risk groups than the low-risk groups in the training cohort (35.1% vs. 77.6%, 25.4% vs. 71.6%, 20.5% vs. 64.7%), the control cohort (23.9% vs. 68.0%, 12.4% vs. 50.2%,

0% vs. 35.3%), as well as the adjuvant HAIC cohort (44.9% vs. 69.9%, 0% vs. 59.5%, 0% vs. 52.4%). Besides, we further compared the RFS among the high-risk group in the adjuvant HAIC cohort, the low-risk group in the adjuvant HAIC cohort, and the control cohort (Fig. 4D). The median RFS for the low-risk group of the adjuvant HAIC cohort was significantly longer than that of the control cohort (P < 0.001). However, there was no statistically significant difference observed between the high-risk group receiving adjuvant HAIC and the control group (P = 0.61).

# Biological processes associated with the imaging-based model

Of the 61 included patients, 6 were classified as high risk and the remaining 55 patients as low risk. The patient characteristics in the RNA-seq sample are shown in Table S5, Supplemental Digital Content 2, http://links.lww.com/JS9/D50. The RNA sequencing data analysis and bioinformatic analysis were detailed in supplement material Appendix S1, Supplemental Digital Content 2, http://links.lww.com/JS9/D50. A total of 1316 annotated genes were identified in the RNA-seq data analysis by their association with the imaging-based model, including 875 up-regulated genes and 441 down-regulated genes (Fig. 5A). Enrichment analysis revealed that differentially expressed genes were mainly involved in the immune-regulating signal transduction, such as antigen processing and presentation, inflammatory mediator regulation of TRP channels, and the TGF-β signaling pathway (Fig. 5B, C).

#### **Discussion**

Adjuvant HAIC therapy has been previously shown to confer a survival benefit in MVI-positive HCC patients. However, being a highly heterogeneous tumor, relying solely on MVI as the criterion for patient selection of adjuvant HAIC treatment was deemed inappropriate. In this large multicenter cohort study, we demonstrated the prognostic model based on four independent imaging features could help to effectively discriminate patients with MVI, thereby providing additional insights for optimizing the treatment strategy of adjuvant HAIC therapy. Besides, our findings based on RNA-seq data analysis uncovered that differentially expressed genes were found to commonly be involved in inflammatory response regulation, and immune regulation.

Due to the extremely high recurrence rate, effective and welltolerated adjuvant treatment strategies for HCC are urgently needed<sup>[5]</sup>. Previous studies investigated potential options, such as interferon<sup>[16]</sup>, stereotactic body radiotherapy<sup>[17]</sup>, systemic chemotherapy<sup>[18]</sup>, and target therapy like sorafenib<sup>[19]</sup>, which have yielded inconclusive results in terms of both efficacy and safety. In recent years, immune checkpoint blockade has shown remarkable efficacy in HCC, leading to the exploration of various immunotherapy-based approaches in the adjuvant setting<sup>[20]</sup>. The preliminary findings of IMbrave050 have demonstrated that adjuvant treatment with atezolizumab plus bevacizumab (A+T) significantly improves the RFS in patients at high risk of disease recurrence following curative resection or ablation<sup>[21]</sup>. However, the prolonged treatment duration, the significant financial burden as well as the potential adverse effect associated with A + T pose a substantial challenge in the clinical management of HCC. Additionally, intrahepatic recurrence occurs more frequently due to intrahepatic dissemination or micro-metastases of the primary cancer cell, and it is widely acknowledged that the presence of

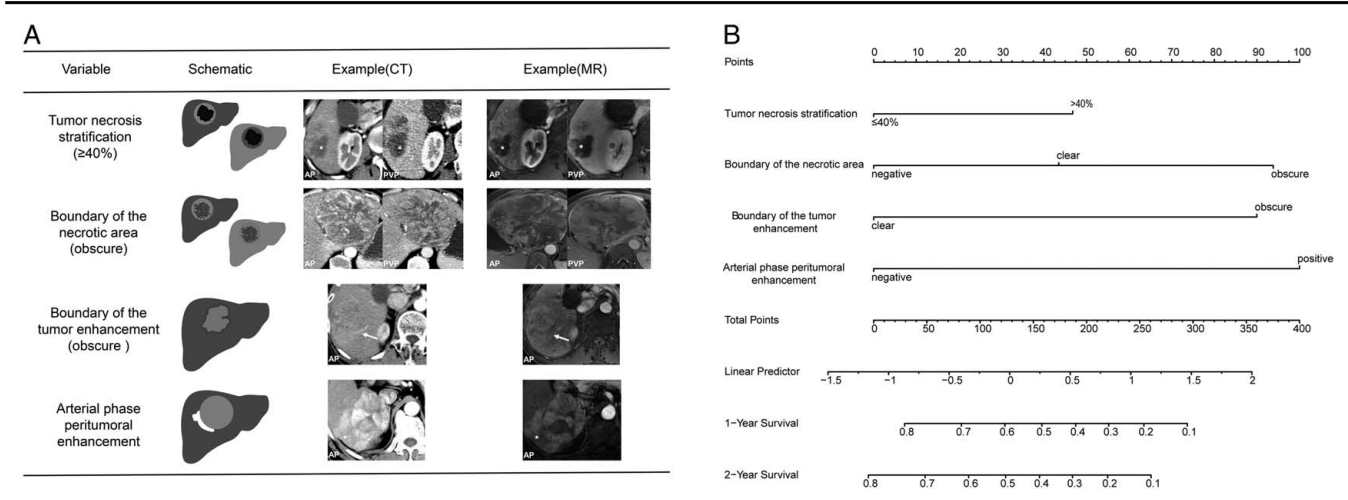


Figure 2. Schematic drawing and nomogram of the prognostic model for recurrence-free survival. Schematic drawings and images of additional features of hepatocellular carcinoma on computed tomography (CT)/magnetic resonance (MR) (A). Nomogram for recurrence-free survival of hepatocellular carcinoma patients with microvascular invasion undergoing curative resection (B). AP, arterial phase; PVP, portal venous phase.

MVI significantly contributes to the risk of recurrence<sup>[22,23]</sup>. Thus, our previous study demonstrated that HCC patients confirmed with MVI-positive after curative resection can derive a survival benefit from adjuvant HAIC treatment. Local adjuvant

therapy through continuous infusion of FOLFOX drugs could ensure adequate local drug concentration in the liver, thereby eradicating micro-metastases. However, MVI-positive HCC patients are also a highly heterogeneous group<sup>[8,24]</sup>, and there

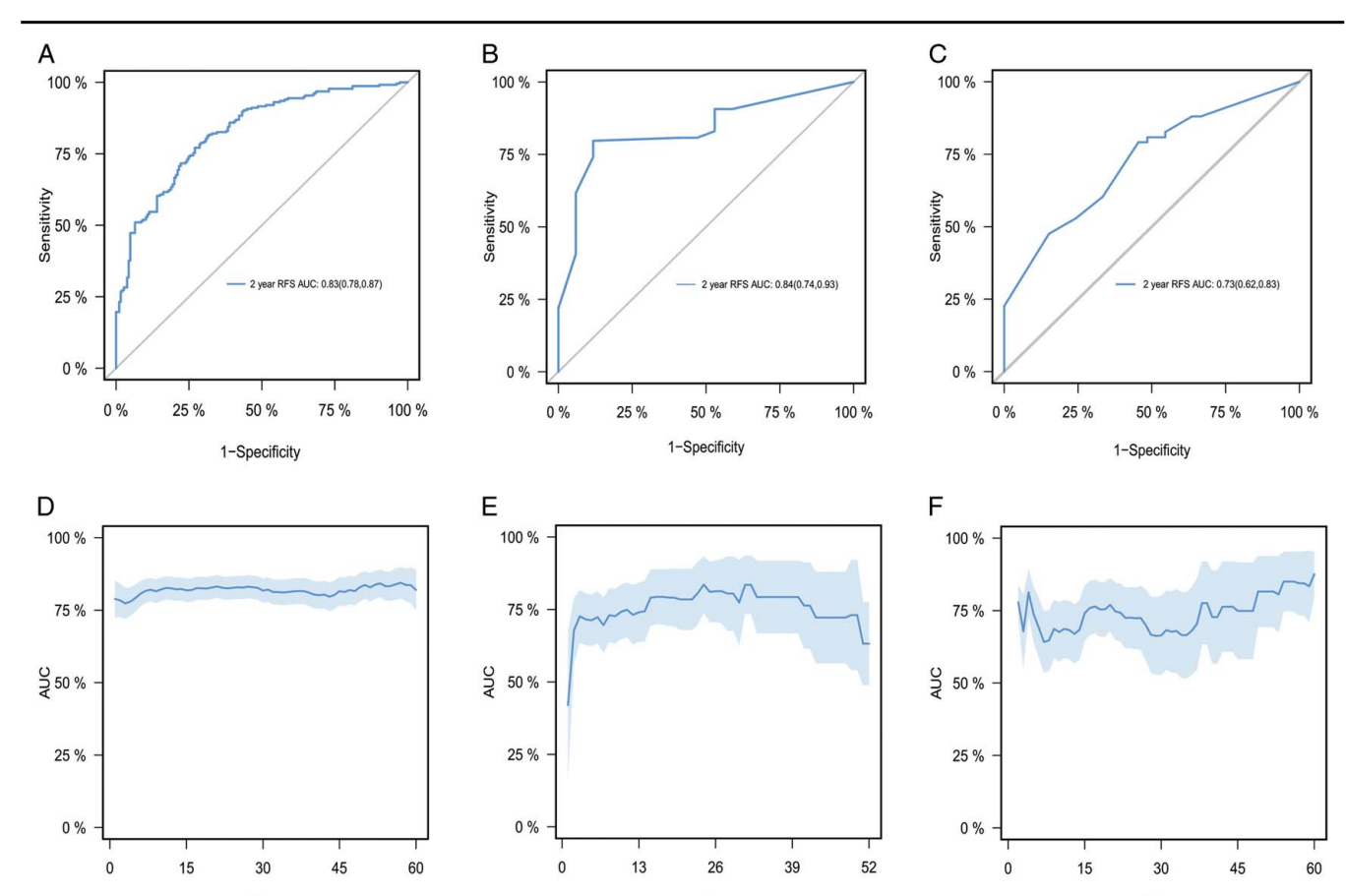


Figure 3. Assessment of the Product for the ability to predict recurrence. Areas under the receiver operating characteristic curve (AUROC) for the ability to predict recurrence. Areas under the receiver operating characteristic curve (AUROC) for the ability to predict recurrence. Areas under the receiver operating characteristic curve (AUROC) adjuvant HAIC cohort (n = 143). AUROCs are reported with 95% CI in parentheses. Time-dependent area under the receiver operating characteristic curve (tdAUROC) value over time of the model for the (D) training cohort, (E) control cohort, and (F) adjuvant HAIC cohort. HAIC, hepatic arterial infusion chemotherapy. RFS, recurrence-free survival.

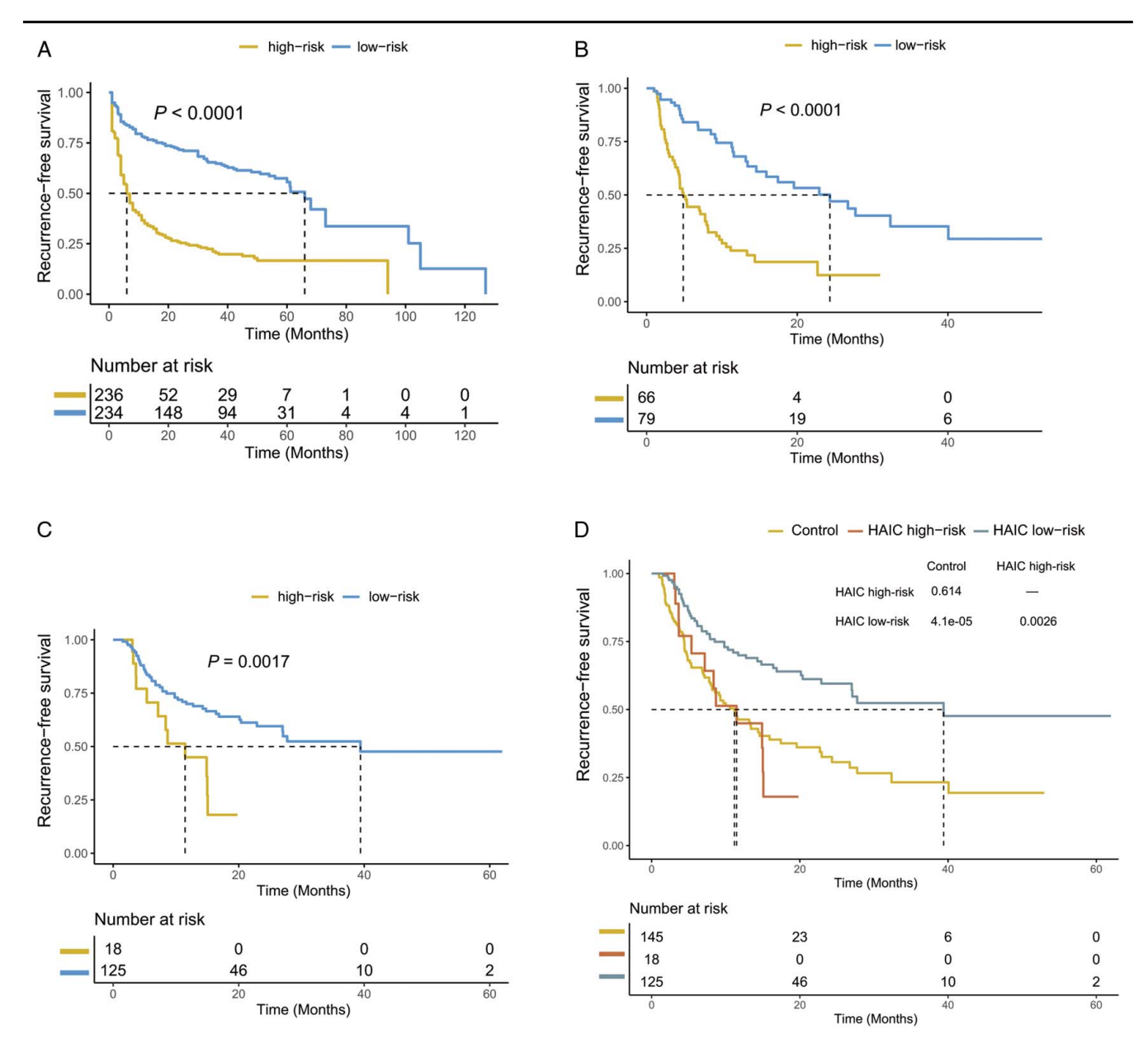
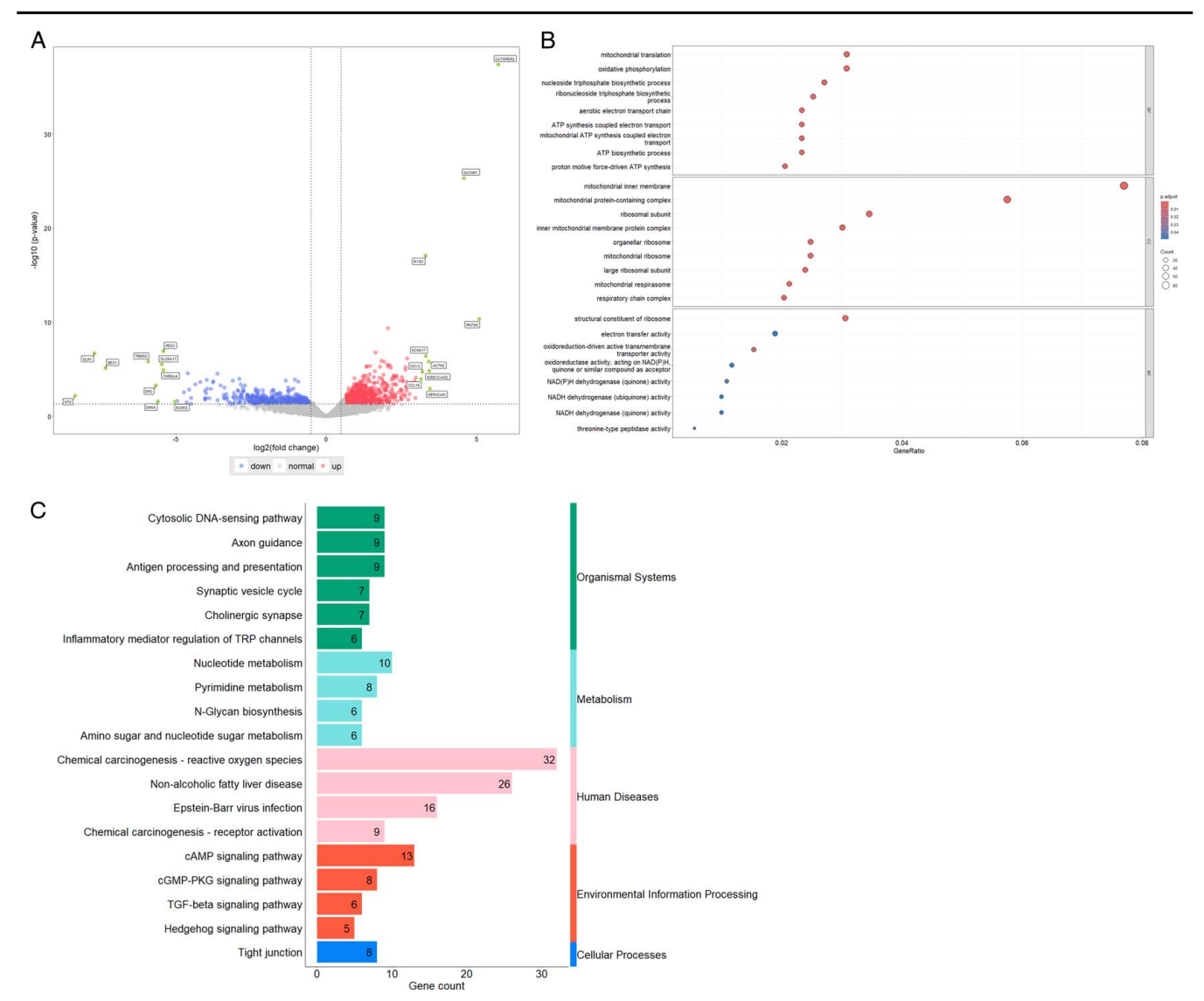


Figure 4. Performance of the nomogram for prognosis prediction in the different cohorts. Kaplan–Meier recurrence-free survival curves (RFS) of different risk groups in (A) training cohort, (B) control cohort, and (C) adjuvant HAIC cohort for the entire follow-up period since curative hepatic resection. Kaplan–Meier RFS curves between the adjuvant HAIC risk groups and control cohort (D). HAIC, hepatic arterial infusion chemotherapy.

exists a subset of individuals who do not derive significant benefit from adjuvant HAIC treatment, particularly given the underlying liver disease present in almost all patients. Therefore, it is imperative to identify MVI-positive patients who exhibit no response to adjuvant HAIC treatment and to perform further risk stratification for them.

Preoperative radiographic examination is an indispensable part of clinical practice. Over the past decade, its significance has rapidly evolved from being a primary diagnostic tool to assuming a predominant position in personalized treatment scenarios<sup>[25]</sup>. HCC patients exhibit distinct microscopic molecular subtypes, which may contribute to diverse pathological presentations and consequently result in varied tumor imaging characteristics<sup>[26–28]</sup>. By integrating four imaging features, namely arterial phase

peritumoral enhancement, boundary of the tumor enhancement, tumor necrosis stratification, and boundary of the necrotic area, this study successfully categorized HCC patients with MVI-positive in terms of RFS and further stratified those who received adjuvant HAIC treatment into two distinct groups, in which those who were classified as the high-risk group suffer similar RFS with those who just received active routine follow-up after curative resection (median RFS, 11.46 vs. 11.16 months, P = 0.61). Thus, additional evaluation of the imaging features is an inexpensive, readily available, simplified approach in clinical practice, serving the purpose of highlighting the heterogeneity of MIV-positive HCC patients and providing more comprehensive prognostic information for those undergoing adjuvant HAIC treatment after curative resection.



**Figure 5.** RNA-seq data analysis associated with the prognostic model. (A) The volcano plot shows the differentially expressed genes in the low-risk group compared with the high-risk group. (B) The bubble plots show the results of the analysis when using Gene Ontology (GO) between the low-risk group and the high-risk group. (C) The bar diagram of Kyoto Encyclopedia of Genes and Genomes (KEGG) analysis shows representative pathway names on the *y*-axis and the percentage of differentially expressed genes between the low-risk group and high-risk group in that pathway on the *x*-axis.

The elucidation of the biological significance underlying the patterns observed in the imaging-based model remains a formidable scientific challenge. Gene enrichment analysis conducted in this study revealed that differentially expressed genes between the high-risk and low-risk groups were commonly associated with immune-regulating signal transduction pathways. The extent of necrosis serves as an indicator for both tumor hypoxia and the invasive growth pattern<sup>[29]</sup>, while the formation and alteration of tumor microvessels and necrosis can directly induce hemodynamic changes and infiltration of macrophages<sup>[30]</sup>. Additionally, the boundary between malignant cells in the outermost circle of HCC and surrounding non-malignant cells is associated with hypoxia, regulation of inflammatory mediators, and immune evasion<sup>[31]</sup>. Notably, the transforming growth factor  $\beta$  (TGF- $\beta$ ) signaling pathway also plays a crucial role in promoting tumor metastasis, immune evasion of tumor cells, and angiogenesis during malignancy progression<sup>[32]</sup>. Specifically, TGF- $\beta$  stimulates blood vessel formation, leading to the development of fragile tumor microvessels that are prone to hypoxia and necrosis. Therefore, it is plausible that the regulation of inflammatory response and immune signaling pathways within the tumor microenvironment are linked to infiltrative growth patterns as reflected by radiological features.

Our study had certain limitations. Firstly, the retrospective cohort used for training in our study may introduce inherent biases. Secondly, a majority of the enrolled patients exhibited hepatitis B virus infection. Therefore, further validation is required before applying the model to HCC patients from different ethnic groups and hepatitis backgrounds. In addition, we exclusively employed qualitative image data in this study and intend to investigate the potential role of quantitative data such as radiomics or deep learning in the future. Due to the retrospective

study with a limited sample size and tissue samples, it is inevitable that deviation in RNA-seq analysis will occur in the analysis results. In addition, there are deficiencies for those with MVI-negative, as well as other pathological indicators, which were not included in our study. In the follow-up study, we will increase the sample size and conduct a prospective study to further verify the results and explore the comparison with multiple pathological factors and imaging parameters.

In conclusion, we have developed a novel imaging-based model to depict the heterogeneity of MVI-positive HCC patients, thereby facilitating the identification of patients who would potentially derive benefit from adjuvant HAIC treatment.

#### **Ethical approval**

This investigation received approval from the local Research Ethics Committees Sun Yat-sen University Cancer Center Institutional Review Board. The reference number is B2021-214-Y02.

#### Consent

The informed consent was duly waived from all participating patients due to the retrospective study.

#### Source of funding

This study was supported by grants from the National Natural Science Foundation of China (No. 82203111) and the Science and Technology Projects in Guangzhou (No. 2023A04J1781, No. 2024A04J4081).

## **Author contribution**

Concept and design: L.L., L.M. Data collection: L.M., C.Z., Y.W., K.X., S.L., Z.G., S.L., S.Y., X.L., C.Z., J.H., J.Z., M.G., B.X. Experiments and procedures: L.L., C.X., W.W., R.G. Statistical analysis: L.M., C.Z., Y.W., L.L. Writing of article: all authors. Critical revision and final approval of the manuscript: all authors.

### Conflicts of interest disclosure

All authors declared that they do not have anything to disclose regarding funding or conflict of interest with respect to this manuscript.

# Research registration unique identifying number (UIN)

Researchregistry.com researchregistry10114. Research Registry (knack.com).

#### Guarantor

Lianghe Lu, Chuanmiao Xie, Wei Wei, and Rongping Guo are the guarantors.

#### **Data availability statement**

For scientific reasons, raw data may be obtained with the permission of the corresponding author.

#### Provenance and peer review

Not commissioned, externally peer-reviewed.

#### **Acknowledgement**

The authors thank to Jibin Li for the statistical guidance.

#### References

- Sung H, Ferlay J, Siegel RL, et al. Global Cancer Statistics 2020: GLOBOCAN Estimates of Incidence and Mortality Worldwide for 36 Cancers in 185 Countries. CA Cancer J Clin 2021;71:209–49.
- [2] Forner A, Reig M, Bruix J. Hepatocellular carcinoma. Lancet 2018;391: 1301–14.
- [3] Devarbhavi H, Asrani SK, Arab JP, et al. Global burden of liver disease: 2023 update. J Hepatol 2023;79:516–37.
- [4] Zeng Z-M, Mo N, Zeng J, et al. Advances in postoperative adjuvant therapy for primary liver cancer. World J Gastrointest Oncol 2022;14: 1604–21.
- [5] Zhang W, Zhang B, Chen XP. Adjuvant treatment strategy after curative resection for hepatocellular carcinoma. Front Med 2021;15:155–69.
- [6] Li SH, Mei J, Cheng Y, et al. Postoperative adjuvant hepatic arterial infusion chemotherapy with FOLFOX in hepatocellular carcinoma with microvascular invasion: a multicenter, phase III, randomized study. J Clin Oncol 2023;41:1898–908.
- [7] Li S, Mei J, Wang Q, et al. Postoperative adjuvant transarterial infusion chemotherapy with FOLFOX could improve outcomes of hepatocellular carcinoma patients with microvascular invasion: a preliminary report of a phase III, randomized controlled clinical trial. Ann Surg Oncol 2020;27: 5183–90.
- [8] Portolani N, Baiocchi GL, Molfino S, et al. Microvascular infiltration has limited clinical value for treatment and prognosis in hepatocellular carcinoma. World J Surg 2014;38:1769–76.
- [9] Beaufrere A, Caruso S, Calderaro J, et al. Gene expression signature as a surrogate marker of microvascular invasion on routine hepatocellular carcinoma biopsies. J Hepatol 2022;76:343–52.
- [10] Hartmann K, Šadée CY, Šatwah I, et al. Imaging genomics: data fusion in uncovering disease heritability. Trends Mol Med 2023;29:141–51.
- [11] Tomaszewski MR, Gillies RJ. The biological meaning of radiomic features. Radiology 2021;298:505–16.
- [12] Segal E, Sirlin CB, Ooi C, et al. Decoding global gene expression programs in liver cancer by noninvasive imaging. Nat Biotechnol 2007;25: 675–80.
- [13] Monzawa S, Ichikawa T, Nakajima H, et al. Dynamic CT for detecting small hepatocellular carcinoma: usefulness of delayed phase imaging. AJR Am J Roentgenol 2007;188:147–53.
- [14] Kong C, Zhao Z, Chen W, et al. Prediction of tumor response via a pretreatment MRI radiomics-based nomogram in HCC treated with TACE. Eur Radiol 2021;31:7500–11.
- [15] Mathew G, Agha R, Albrecht J, et al. STROCSS 2021: Strengthening the reporting of cohort, cross-sectional and case-control studies in surgery. Int J Surg 2021;96:106165.
- [16] Ikeda K, Arase Y, Saitoh S, et al. Interferon beta prevents recurrence of hepatocellular carcinoma after complete resection or ablation of the primary tumor—a prospective randomized study of hepatitis C virusrelated liver cancer. Hepatology 2000;32:228–32.
- [17] Shi C, Li Y, Geng L, et al. Adjuvant stereotactic body radiotherapy after marginal resection for hepatocellular carcinoma with microvascular invasion: a randomised controlled trial. Eur J Cancer 2022;166:176–84.
- [18] Li J, Xing J, Yang Y, et al. Adjuvant 131I-metuximab for hepatocellular carcinoma after liver resection: a randomised, controlled, multicentre, open-label, phase 2 trial. Lancet Gastroenterol Hepatol 2020;5:548–60.
- [19] Bruix J, Takayama T, Mazzaferro V, et al. Adjuvant sorafenib for hepatocellular carcinoma after resection or ablation (STORM): a phase

- 3, randomised, double-blind, placebo-controlled trial. Lancet Oncol 2015;16:1344–54.
- [20] Brown ZJ, Greten TF, Heinrich B. Adjuvant treatment of hepatocellular carcinoma: prospect of immunotherapy. Hepatology 2019;70:1437–42.
- [21] Hack SP, Spahn J, Chen M, et al. IMbrave 050: a Phase III trial of atezolizumab plus bevacizumab in high-risk hepatocellular carcinoma after curative resection or ablation. Future Oncol 2020;16:975–89.
- [22] Lim KC, Chow PK, Allen JC, et al. Microvascular invasion is a better predictor of tumor recurrence and overall survival following surgical resection for hepatocellular carcinoma compared to the Milan criteria. Ann Surg 2011;254:108–13.
- [23] Lee S, Kang TW, Song KD, et al. Effect of microvascular invasion risk on early recurrence of hepatocellular carcinoma after surgery and radiofrequency ablation. Ann Surg 2021;273:564–71.
- [24] Huang C, Zhu XD, Ji Y, et al. Microvascular invasion has limited clinical values in hepatocellular carcinoma patients at Barcelona Clinic Liver Cancer (BCLC) stages 0 or B. BMC cancer 2017;17:58.
- [25] Liu Z, Duan T, Zhang Y, et al. Radiogenomics: a key component of precision cancer medicine. Br J Cancer 2023;129:741–53.

- [26] Meng X-P, Tang T-Y, Zhou Y, et al. Predicting post-resection recurrence by integrating imaging-based surrogates of distinct vascular patterns of hepatocellular carcinoma. JHEP Rep 2023;5:100806.
- [27] Feng Z, Li H, Zhao H, et al. Preoperative CT for characterization of aggressive macrotrabecular-massive subtype and vessels that encapsulate tumor clusters pattern in hepatocellular carcinoma. Radiology 2021;300:219–29.
- [28] Zhang P, Ono A, Fujii Y, et al. The presence of vessels encapsulating tumor clusters is associated with an immunosuppressive tumor microenvironment in hepatocellular carcinoma. Int J Cancer 2022;151:2278–90.
- [29] Rhee H, Chung T, Yoo J, et al. Gross type of hepatocellular carcinoma reflects the tumor hypoxia, fibrosis, and stemness-related marker expression. Hepatol Int 2020;14:239–48.
- [30] Leek R, Landers R, Harris A, *et al.* Necrosis correlates with high vascular density and focal macrophage infiltration in invasive carcinoma of the breast. Br J Cancer 1999;79:991–5.
- [31] Wu R, Guo W, Qiu X, et al. Comprehensive analysis of spatial architecture in primary liver cancer. Sci Adv 2021;7:eabg3750.
- [32] Gough N, Xiang X, Mishra L. TGF-β signaling in liver, pancreas, and gastrointestinal diseases and cancer. Gastroenterology 2021;161:434–452.e415.